



Published in final edited form as:

IEEE Trans Biomed Eng. 2012 July ; 59(7): 2030–2039. doi:10.1109/TBME.2012.2196699.

## Aggregate Input Output Models of Neuronal Populations

**Shreya Saxena\***

Department of Electrical Engineering and Computer Sciences, Massachusetts Institute of Technology, Cambridge MA, 02139

**Marc H. Schieber**

Department of Neurology, Cognitive Behavioral Neurology, University of Rochester Medical Center, Rochester NY, 14642

**Nitish V. Thakor [Fellow, IEEE] and Sridevi V. Sarma [Member, IEEE]**

Department of Biomedical Engineering, Johns Hopkins University, Baltimore MD, 21218.

### Abstract

An extraordinary amount of electrophysiological data has been collected from various brain nuclei to help us understand how neural activity in one region influences another region. In this paper, we exploit the point process modeling (PPM) framework and describe a method for constructing aggregate input-output (IO) stochastic models that predict spiking activity of a population of neurons in the “output” region as a function of the spiking activity of a population of neurons in the “input” region. We first build PPMs of each output neuron as a function of all input neurons, and then cluster the output neurons using the model parameters. Output neurons that lie within the same cluster have the same functional dependence on the input neurons. We first applied our method to simulated data, and successfully uncovered the predetermined relationship between the two regions. We then applied our method to experimental data to understand the input-output relationship between motor cortical neurons and (i) somatosensory and (ii) premotor cortical neurons during a behavioral task. Our aggregate IO models highlighted interesting physiological dependencies including relative effects of inhibition/excitation from input neurons and extrinsic factors on output neurons.

### I. INTRODUCTION

THE communication between any two sites of the brain is a complicated process involving many synapses. In order to uncover the underlying structure of this communication, it is important to have a tractable input-output (IO) model that predicts spiking activity of neurons in one region, henceforth referred to as *output neurons*, as a function of the spiking activity of neurons in another region, henceforth referred to as *input neurons*.

A vast amount of data is being recorded simultaneously from neurons located in different brain structures [1], [2]. Second order statistics such as cross-correlation and coherence measures are often used to gauge the relationship between the spiking activity of pairs of

neurons [3], [4]. However, these are limited measures that provide snapshots of interactions between individual neurons from different regions. They shed insight into neural communication but do not explicitly provide a model that predicts how one region's activity impacts another.

Different models have been proposed over the years to gauge the effect of neurons in one site on neurons in another. Many are biophysical-based models, which characterize the nonlinear dynamics of ionic conductances and synapses between neurons [5], [6]. Although useful in understanding underlying physiology and mechanisms of spike generation, these models become intractable for analysis of populations of neurons. Furthermore, they require the estimation of a large number of parameters that cannot be easily fit via extracellular recordings.

Point process models (PPMs) of neural spike train data are well-suited to characterize dynamics of individual neurons as a function of environmental and intrinsic factors and have been used to study a wide range of neural systems [7]–[12]. These models are predictive, i.e. one can feed any set of spike train inputs into them, and obtain a set of spike train outputs that obey the stochastic distribution. The PPM model parameters provide us direct information on the effect of the input neurons on the output neurons, and are thus simple to analyze. However, with the recent advance in the ability to simultaneously record a large number of single units in different brain structures, we need a systematic method to be able to parse through this data. Instead of studying a large number of individual IO models, we would like to analyze a tractable reduced-order representation of the effects of spiking activity in one region on the spiking activity in another region.

We propose a method to construct data-driven aggregate IO models (Fig. 1B), that characterize the probability distribution of the spiking activity of a population of output neurons conditioned on the spiking activity of input neurons, i.e.  $\Pr(\mathbf{y}|\mathbf{u})$ . Specifically, we construct the aggregate models in three steps: (i) build individual IO models for each output neuron as a function of *all* input neurons, (ii) cluster the output neurons using the individual model parameters, and (iii) build aggregate IO models for each cluster of output neurons. Note that though we use the term 'neurons' in this study, we can also perform the same analysis with multi-unit activity, as we show in Section IV-C.

Fig. 1A shows an original system of  $n$  inputs and  $m$  outputs, which is reduced to an aggregated system of  $n$  inputs and  $K$   $m$  outputs in Fig. 1B. A transfer matrix representation of an example is shown in Fig 1C and D. We see that this method helps us reduce the number of IO models of all the output neurons receiving inputs from all the input neurons from  $m$  to  $K$ .

We applied our method to simulated data, as well as data sets from sensory motor, premotor, and motor cortex. For the simulated data, we defined physical and physiological connections between 3 input neurons and 45 output neurons in such a manner that gave rise to 3 clusters with unique IO relationships. Our method successfully uncovered both the physical structure and the spiking dynamics.

We then applied our method to groups of neurons in the Somatosensory Cortex (S1) simultaneously recorded with neurons in the Primary Motor Cortex (M1) neurons in a primate performing a set of four different behavioral tasks. We obtained 2 clusters of M1 neurons which had different dependencies on the S1 input neurons. In particular, all M1 neurons experienced a significant excitatory effect from one S1 neuron with a short latency. A subset of the M1 neurons exhibit an inhibition from another S1 neuron with a longer latency, which may arise in order to balance the previous excitation.

Finally, we applied our method to analyse the activity of the M1 neurons as a function of the activity of ventral Premotor Cortex (PMv) during the same experiment. We uncovered 4 different clusters of M1 neurons with a different set of PMv input neurons; 2 of these clusters showed M1 activity which was task specific, while the other 2 did not show any task specificity. The task-specific M1 clusters received a combination of significant inhibitory as well as excitatory inputs from the PMv neurons. This suggests a non-trivial relationship between the M1 and PMv neurons, resulting in a planned task-specific movement.

## II. METHODS

### A. Point Process Estimation

A point process is a series of 0-1 random events that occur on a continuum such as space or time. For a neural spike train, the 1s are individual spike times and the 0s are the times at which no spikes occur. To define a point process model of neural spiking activity, we consider an observation interval  $(0; T]$  and let  $N(t)$  be the number of spikes counted in interval  $(0; t]$  for  $t \in (0; T]$ : A point process model of a neural spike train can then be completely characterized by its conditional intensity function (CIF), defined as

$$\lambda(t|H_t) \triangleq \lim_{\Delta \rightarrow 0} \frac{Pr(N(t+\Delta) - N(t) = 1 | H_t)}{\Delta}, \quad (1)$$

where  $H_t$  denotes the spiking history up to time  $t$ . It follows from (1) that the probability of a single spike in a small interval  $(t; t + \Delta]$  is approximately

$$Pr(\text{spike in } (t, t+\Delta]) \simeq \lambda(t|H_t) \Delta. \quad (2)$$

Details can be found in [13], [14]. The CIF generalizes the rate function of a Poisson process to a rate function that is history dependent. Because the CIF completely characterizes a spike train, defining a model for the CIF defines a model for the spike train [13], [15].

For our analyses, we use the generalized linear model (GLM) to define our CIF models by expressing for each neuron, the log of its CIF in terms of the neuron's spiking history and the relevant input neurons' spiking history. The GLM is an extension of the multiple linear regression model in which the variable being predicted, in this case spike times, need not be Gaussian [16]. GLM also provides an efficient computational scheme for model parameter estimation and a likelihood framework for conducting statistical inferences. Therefore, we compute model parameters from the data via maximum likelihood estimation [15].

## B. Individual Input Output Models

To obtain an aggregate IO models between two populations of neurons, we first build individual IO models by estimating the CIF of each output neuron as a function of all the input neurons. These individual models take the multiplicative structure shown in (3) for a given output neuron,  $j$  for  $j \in [1, \dots, m]$ , and all of the input neurons  $i = 1, 2, \dots, n$ . We denote the spike train time series for output neuron  $j$  as  $y_j(t)$  and input neuron  $i$  as  $u_i(t)$ .

$$\lambda_j \left( t | H_t^{y_j}, H_t^u, \Theta_j \right) = e^{\alpha_j} \cdot \lambda^O \left( t | H_t^{y_j}, \Theta_j \right) \cdot \lambda^I \left( t | H_t^u, \Theta_j \right) \quad (3)$$

Here,  $\lambda^O$  represents the contribution of the output neuron's own spiking history,  $H_t^{y_j}$ , since neurons are known to be affected by their own spiking history (e.g. refractory periods, bursts, oscillations).  $\lambda^I$  represents the contribution due to the input neurons' spiking histories,  $H_t^u$  and  $e^{\alpha_j}$  is a history-independent term that captures the background firing rate. The parameter vector  $\Theta_j$  is to be estimated from data individually for each output neuron  $y_j$ .

Expressing the rate as a product of the different components allows one to assess how much each component contributes to the spiking propensity of the neuron [9], [11]. If, for example, the spiking history of both the input neurons,  $H_t^u$  and the output neuron,  $H_t^{y_j}$ , are not associated with the output neurons' response, then  $\lambda^I$  and  $\lambda^O$  will be very close to 1, and (3) reduces to  $\lambda_j \left( t | H_t^{y_j}, H_t^u, \Theta_j \right) = e^{\alpha_j}$  a standard Poisson process.

These functions are modeled using the GLM framework, i.e.,

$$\begin{aligned} \log \lambda^O \left( t | H_t^{y_j}, \Theta_j \right) &= \sum_{r=1}^{D_O} \gamma_r^j N_{t-r}^{y_j} \\ \log \lambda^I \left( t | H_t^u, \Theta_j \right) &= \sum_{i=1}^n \sum_{r=1}^{D_I} \beta_r^{i,j} N_{t-r}^{u_i}, \end{aligned} \quad (4)$$

where  $N_{t-r}^{y_j}$  and  $N_{t-r}^{u_i}$  denote the number of spikes generated by output neuron  $j$  and input neuron  $i$ , respectively, in  $[t-r, t-(r-1))$  ms with  $r$  chosen differently for each case study. Each summation is taken over  $D_O$  and  $D_I$  steps, where  $D_O$  and  $D_I$  are the extent of history of the output spike train and input spike trains respectively, as considered as having

an effect on each output neuron. The parameter vector  $\Theta_j = \left[ \alpha_j, \left\{ \gamma_r^j \right\}_{r=1}^{D_O}, \left\{ \left\{ \beta_r^{i,j} \right\}_{r=1}^{D_I} \right\}_{i=1}^n \right]$  is estimated from data via maximum likelihood estimation [15].

## C. Clustering

We use the K-means clustering algorithm [17] to group the parameter vectors  $\Theta_1, \Theta_2, \dots, \Theta_m$  of the individual models to see if an underlying structure between the input and output neurons can be uncovered. In K-means clustering, the sum of the squared Euclidean distances of all the parameter vector points to their respective cluster centroids is minimized. The initial cluster centroids are chosen at random, but we iterate at least 20 times with a new set of initial centroids in order to avoid stopping in local minima. Silhouette coefficients [18]

are then computed for each  $\Theta_j$  to measure the intra-cluster homogeneity and cluster-to-cluster heterogeneity according to the formula:

$$S_j = \frac{\min_k (d_j(k)) - c_j}{\max(c_j, \min_k (d_j(k)))} \quad k \in 1, 2, \dots, K, \quad (5)$$

where  $c_j$  is the average distance from  $\Theta_j$  to the other parameter vectors in its own cluster, and  $d_j(k)$  is the average distance from  $\Theta_j$  to parameter vectors in *another* cluster  $k$ . The optimal number of clusters  $K$  is chosen after computing the silhouette coefficients for different values of  $K$ , and taking that which yields the maximum average silhouette value [18].

#### D. Aggregate Input Output Models

After clustering, we construct aggregate IO models for each cluster for  $k = 1, 2, \dots, K$  separately. We take all the output neurons whose individual models belong to cluster  $k$  and treat their spike trains as different trial sessions of a single neuron or a single “unit”. Specifically, we concatenate all the spike trains of the output neurons in cluster  $k$ , and define the concatenated spike train as  $y_k$ . We then estimate one parameter vector of the aggregate model  $\bar{\Theta}_k$  using the input neurons’ spike trains  $u$ , and the output neuron’s spike train  $y_k$ , i.e. with the CIF detailed in (6)

$$\lambda_k \left( t | H_t^{y_k}, H_t^u, \bar{\Theta}_k \right) = e^{\bar{\alpha}_k} \cdot \lambda^{y_k} \left( t | H_t^{y_k}, \bar{\Theta}_k \right) \cdot \lambda^u \left( t | H_t^u, \bar{\Theta}_k \right) \quad (6)$$

The components in (6) are each a GLM with the following functions:

$$\begin{aligned} \log \lambda^{y_k} \left( t | H_t^{y_k}, \bar{\Theta}_k \right) &= \sum_{r=1}^{D_O} \bar{\gamma}_r^k N_{t-r}^{y_k} \\ \log \lambda^u \left( t | H_t^u, \bar{\Theta}_k \right) &= \sum_{i=1}^n \sum_{r=1}^{D_I} \bar{\beta}_r^i N_{t-r}^{u_i}, \end{aligned} \quad (7)$$

where the  $\bar{\beta}_s$  no longer depend on specific output neuron  $j$ . We note that the  $\bar{\beta}_s$  depend on the cluster  $k$ , but we omit this in our notation for a simpler read.

Finally, we analyze the parameter vectors for each aggregate model,  $\bar{\Theta}_1, \bar{\Theta}_2, \dots, \bar{\Theta}_K$ , to infer the effect of groups of input neurons on groups of output neurons in each cluster [11], [19], [20]. The clustering reduces the number of possible connections and the number of models to consider in order to characterize the input-output dynamics of the two populations of neurons in consideration. We also calculate the order of model reduction that we achieved:

$$\rho = \frac{\# \text{IO models in original representation}}{\# \text{IO models in aggregate representation}} = \frac{K}{m} \quad (8)$$

### III. APPLICATION TO SIMULATED DATA

Before analyzing real data sets, we apply and validate our methodology on simulated data. We define specific physical connections and physiological dependencies for three populations of neurons and use our method to uncover these IO relationships.

#### A. Physical and Physiological Connections

We simulated the activity of 3 input neurons and 45 output neurons with physical connections shown in Figure 2A. Note that input neurons 1 and 2 simultaneously affect output neurons 1 – 30, though input neuron 1 has separate effects on output neurons 1 – 15 as compared to output neurons 16 – 30. Input neuron 3 is the only neuron that affects output neurons 31 – 45. The physiological dependencies between these neurons are described by equations (9) and (10) where  $t$  is discretized into 1 millisecond bins.

$$\forall j \in [1, 15]:$$

$$\log(\lambda^{y_j}(t|\tilde{\Theta}_j)) = \tilde{\alpha}_0 + \tilde{\gamma}_R N_{t-1}^{y_j} + \sum_{l=1}^{51} \tilde{\beta}_{1a}(l) N_{t-1}^{u_1} + \sum_{l=1}^{51} \tilde{\beta}_2(l) N_{t-1}^{u_2} \quad (9)$$

$$\forall j \in [16, 30]:$$

$$\log(\lambda^{y_j}(t|\tilde{\Theta}_j)) = \tilde{\alpha}_0 + \tilde{\gamma}_R N_{t-1}^{y_j} + \sum_{l=1}^{51} \tilde{\beta}_{1b}(l) N_{t-1}^{u_1} + \sum_{l=1}^{51} \tilde{\beta}_2(l) N_{t-1}^{u_2} \quad (10)$$

$$\forall j \in [31, 45]:$$

$$\log(\lambda^{y_j}(t|\tilde{\Theta}_j)) = \tilde{\alpha}_0 + \tilde{\gamma}_R N_{t-1}^{y_j} + \sum_{l=1}^{51} \tilde{\beta}_3(l) N_{t-1}^{u_3} \quad (11)$$

where

$$\begin{aligned} \tilde{\alpha}_0 &= \log(20), \tilde{\gamma}_R = -10^{99} \\ \tilde{\beta}_{1a}(l) &= 2\sin(2\pi \cdot 0.025l) \exp(-0.1l) \\ \tilde{\beta}_{1b}(l) &= -2\sin(2\pi \cdot 0.025l) \exp(-0.1l) \\ \tilde{\beta}_2(l) &= 2\sin(2\pi \cdot 0.025(51-l)) \exp(-0.1(51-l)) \\ \tilde{\beta}_3(l) &= -2\sin(2\pi \cdot 0.025(51-l)) \exp(-0.1(51-l)) \end{aligned} \quad (12)$$

We assumed that the input neurons' spiking activity are mutually independent, and generated their spike trains in a Poisson manner with a refractory period of  $R = 1$  ms, and average firing rates of  $\lambda_1 = \lambda_2 = \lambda_3 = 20$  Hz. The refractory period ensures that there is no spike 1 ms immediately after a spike by allowing a 1 in an activity bin only if the previous bin is empty.

We modeled the output neurons to have either a predominantly excitatory ( $\tilde{\beta}_{1a}, \tilde{\beta}_2$ ) or inhibitory ( $\tilde{\beta}_{1b}, \tilde{\beta}_3$ ) response to the input neurons' spiking activity, as described by the parameters  $\tilde{\beta}_i, i = 1a, 1b, 2, 3$  in equation (12) and as depicted in Fig. 2B. For example, the shape of  $\tilde{\beta}_{1a}$  indicates that at some time bin  $t$ , if input neuron 1 spikes in the time interval  $[t$

$-1; t-15]$ ms, then the probability that an output neuron  $j$  (for  $j = 1; 2; \dots, 15$ ) will spike at time  $t$  *modulates up* by a factor of almost 2. On the other hand, the shape of  $\tilde{\beta}_{1b}$  indicates that at some time bin  $t$ , if input neuron 1 spikes in the time interval  $[t-1, t-15]$ ms, then the probability that an output neuron  $j$  (for  $j = 1, 2, \dots, 15$ ) will spike at time  $t$  *modulates up* by a factor of almost 2.

The output neurons were also modeled to have a refractory period of 1 ms which is enforced by the parameter  $\tilde{\gamma}_R = -10^{99}$ . In particular, if at some time  $t$  neuron  $j$  has a spike at time  $t-1$ , then the probability that neuron  $j$  will spike again in time bin  $t$  is effectively 0. The history independent firing rate was modeled to be  $\tilde{\alpha}_0 = \log(20Hz)$ .

Finally, we added noise to the output spike trains by removing 15% of the spikes from each spike train and inserting these spikes at random times during the entire simulated time interval [21]. We simulated 45 output neurons for 15 seconds each. Spike trains of each output neuron were generated using inverse time rescaling as described in [22], [23].

## B. Analysis of Simulated Data

We first built individual IO models of the output neurons assuming that the CIFs were a function of *all* the inputs, as in (3). Each component was modeled as a GLM (4) which took the following form.

$$\log \lambda^{y_j} (t | H_t^{y_j}, H_t^u, \Theta_j) = \alpha_j + \sum_{r=1}^{70} \gamma_r^j N_{t-r}^{y_j} + \sum_{i=1}^3 \sum_{r=1}^{70} \beta_r^{i,j} N_{t-r}^{u_i} \quad (13)$$

Here,  $\Theta_j = \left[ \alpha_j, \left\{ \gamma_r^j \right\}_{r=1}^{70}, \left\{ \left\{ \beta_r^{i,j} \right\}_{r=1}^{70} \right\}_{i=1}^3 \right]$  We obtained 45 different PPMs, as shown in Fig. 3A.

We then clustered the parameter vectors for all the PPMs using k-means clustering as described in section II-C, and obtained silhouette values for values of  $K = 2; \dots, 9$ . We computed the mean silhouette values for each value of  $K$ , and found that the mean silhouette value is maximized for  $K = 3$ . The first two principal components of the clustered parameter vectors are shown in Fig. 3B, and a schematic of the results is shown in Fig. 3C. Note that the  $\Theta_j$ 's cluster as in the original groups of neurons, i.e.  $\Theta_1, \dots, \Theta_{15}$ , are in a different cluster than  $\Theta_{16}, \dots, \Theta_{30}$ , which are themselves in a different cluster than  $\Theta_{31}, \dots, \Theta_{45}$ .

Finally, we built aggregate IO models based on these results by concatenating all the output spike trains in each cluster  $k = 1; 2$ , and building one model per cluster, as in (6), with

$\bar{\Theta}_k = \left[ \bar{\alpha}_k, \left\{ \bar{\gamma}_r^k \right\}_{r=1}^{70}, \left\{ \left\{ \bar{\beta}_r^{i,k} \right\}_{r=1}^{70} \right\}_{i=1}^3 \right]$  (Fig. 4). These two aggregate IO models show the simultaneous effect of the output neurons' own history as well as the history of the input neurons  $u_1; u_2; u_3$  on the output neurons  $y_1, \dots, y_{15}$  (Fig. 4A), and on the output neurons  $y_{16}, \dots, y_{30}$  (Fig. 4B). In this simulated example, there was a reduction of the number of input-output models from 45 to 3, i.e.,  $\sigma = 15$ . Note that

$\bar{\beta}^{(1,1)} \approx \bar{\beta}_{1a}, \bar{\beta}^{(1,2)} \approx \bar{\beta}_{1b}, \bar{\beta}^{(2,1)} \approx \bar{\beta}_2,$  and  $\bar{\beta}^{(3,3)} \approx \bar{\beta}_3.$  Also note that  $\bar{\beta}^{(3,1)}, \bar{\beta}^{(3,2)}, \bar{\beta}^{(1,3)}$  and  $\bar{\beta}^{(2,3)}$  are not statistically significantly different from 0. Thus we uncovered both the physical and physiological connections detailed in Section III-A.

#### IV. APPLICATION TO PRIMATE DATA FROM THE MOTOR, SOMATOSENSORY, AND PREMOTOR CORTEX

Primary Motor Cortex (M1) neurons are known to receive inputs from various structures. Here, we examine the individual influence of Somatosensory Cortex (S1) and the ventral Premotor Cortex (PMv) neurons on the M1 neurons during a behavioral task.

##### A. Experimental Methods

A male non-human primate (macaca mulatta) was visually cued to reach towards, grasp, and manipulate different objects at different spatial locations. The experimental procedures were performed primarily by Dr. Marc Schieber with Dr. Nitish Thakor; details are in [24] and [2]. Single-unit activity was recorded from multiple floating microelectrode arrays (FMAs, MicroProbes, Gaithersburg, MD) that were implanted in cortical motor areas contralateral to the trained hand. Each FMA consisted of 16 Platinum/Iridium electrodes with tip impedance of 0.5 M, arranged in a 4x4 grid with electrode spacing of 500  $\mu$ m. A total of fourteen FMAs were implanted in the monkey ('monkey X' in [2]), with one array in S1, one in PMv, four in M1. Upper-limb kinematics were simultaneously tracked using a Vicon (Oxford, UK) motion capture system. The task involved reaching towards different objects located in different positions in space after the cue was given, manipulation of these objects for a 1000 ms hold period, and then releasing these objects (Fig. 5). Manipulations involved depressing a pushbutton, pulling a coaxial cylinder, pulling a perpendicularly mounted cylinder (mallet), or rotating a sphere 45°.

We first analyzed the effect of single-unit S1 activity (n=8 neurons) on single-unit M1 neurons (n=58 neurons) during the hold period, where the sensory information may play a large role in M1 activity. We then analyzed the effect of multi-unit PMv activity (39 neurons; n=13 channels) on single-unit M1 neurons during the period from the start of the cue to reach for the objects until the end of movement, where accurate motor planning and consequent movement generation occurs. We consider multi-unit PMv activity as a primary reduction in input space, due to the large number of input PMv neurons. Only spike trains with an average discharge rate  $\geq 10$  spikes/s during the period considered were included in this study.

##### B. S1 to M1

We considered the 8 S1 neurons as inputs and 58 M1 neurons as outputs, with 2 S1 neurons and 15 M1 neurons having firing rates  $\geq 10$  spikes/s during the the hold period. All the trials during the four different tasks were pooled together.

**1) Individual Input Output Models**—We estimated PPMs of the form (14) using recordings of the S1 and M1 to obtain a parameter vector associated with each output neuron. The models were constructed to capture the effects due to the spiking activity of the

output neuron's own history ( $\lambda^O$ ), and the single-unit spiking activity of the S1 neurons ( $\lambda^I$ ). We chose the multiplicative model structure [9], [11],  $\lambda^y = e^a \cdot \lambda^O \cdot \lambda^I$ , where

$$\begin{aligned} \log \lambda^O(t|H_t^{y_j}, \Theta_j) &= \sum_{r=1}^{13} \gamma_r^j N_r^{y_j} \\ \log \lambda^I(t|H_t^u, \Theta_j) &= \sum_{i=1}^2 \sum_{r=1}^{10} \beta_r^{i,j} N_r^{u_i}. \end{aligned} \quad (14)$$

Here,  $H_t^{y_j}$  corresponds to the output neuron's own history, and  $u_i$ , the input, corresponds to the single-unit spiking activity of the  $i$ -th S1 neuron.  $N_r^{y_j}$  or  $N_r^{u_i}$  is the number of spikes fired by the  $j$ -th M1 neuron or  $i$ -th S1 neuron in  $[t - r, t - (r - 1)]$  (in ms) respectively

$$(\tau \text{ varied from 1 to 20 ms}), \text{ and } \Theta_j = \left[ \alpha, \left\{ \gamma_r^j \right\}_{r=1}^{13}, \left\{ \left\{ \beta_r^{i,j} \right\}_{r=1}^{10} \right\}_{i=1}^2 \right].$$

We arrived at the above choice of covariates and the model structure given in (14) through an iterative procedure of testing and refining GLM models until the models' cross-validated KS plots displayed a high goodness-of-fit for each model [25]. In this analysis,  $m = 13$  neurons had a PPM with cross-validated KS statistic  $< 0.2$ .

**2) Clustering**—We clustered the PPM parameter vectors for each M1 neuron using K-means clustering, as described in section II-C. The average silhouette values were computed for  $K = 2, \dots, 12$ . We examined the silhouette values for these clustering attempts, and obtained  $K = 2$  clusters with the maximum average silhouette value, 0.74. The resulting clusters defined a simple set of physiological connections between the S1 and M1 neurons. The first cluster contained the inputoutput model parameters of M1 neurons  $n1, n2$ , while the second cluster contained those of M1 neurons  $n3, \dots, n13$ . In this study, there was a reduction of the number of inputoutput models from 13 to 2, i.e.,  $\rho = 6.5$ .

**3) Aggregate Input Output Models**—Once the clusters were determined, we estimated new aggregate point process models for each S1-M1 cluster by taking as inputs and outputs several trials from the S1 and M1, respectively. PPMs of the form (6) and (7) were constructed (Fig. 6).

The PPM for the first cluster of M1 neurons (Fig. 6A) shows that the neurons in this cluster are strongly inhibited by a spike in the previous 30ms, but the propensity to spike increases up to more than 4 times with a spike in the previous 40 – 90ms. The PPM for the second cluster of M1 neurons (Fig. 6B), however, shows that the neurons are only inhibited by a spike in the previous 10ms, while the propensity to spike increases less than 1.5 times with a spike in the previous 20 – 90ms.

The effect of the two S1 neurons on each of the clusters is varied. S1 neuron  $n1$  is seen to have an excitatory effect on both the clusters of M1 neurons with a delay of 1 to 3 ms, but the excitation is more significant in the first cluster than in the second cluster. S1 neuron  $n2$  has a slightly inhibitory effect on the M1 neurons in the first cluster, whereas it has a slightly excitatory effect on the neurons in the second cluster.

In this study, S1 neuron  $n1$  is seen to have a predominantly excitatory effect on all the M1 neurons with a latency of a couple of milliseconds. This may be a result of direct connections from this S1 neuron to the M1 neurons, with a stronger influence on neurons in cluster 1 as compared to those in cluster 2. Direct activation of the motor cortex by the somatosensory neurons has been noted in rats and mice [26], [27].

Cluster 1 also displays a slight inhibition due to the spiking of S1 neuron  $n2$ , which may be present in order to balance the large excitatory influence of S1 neuron  $n1$ . This shows a potential balancing mechanism to prevent the system from being excessively excited via positive feedback loops from one area to the other [28], [29].

### C. PMv to M1

We now investigate the relationship between PMv and M1 spiking. We considered each of the  $n = 13$  channels ( $\approx 115$  trial sessions per channel) recorded at different depths in PMv as input units and  $m = 21$  output neurons ( $\approx 115$  trial sessions per neuron) in M1 during four different tasks. The neural activity analyzed was in the period from the start of the cue to the end of the movement.

**1) Individual Input Output Models**—We estimated PPMs of the form (15) using recordings of the PMv and M1 to obtain a parameter vector associated with each output neuron. The models were constructed to capture the effects due to the spiking activity of the output neuron's own history ( $\lambda^O$ ), and the multi-unit spiking activity of the PMv channels ( $\lambda^I$ ). We chose the multiplicative model structure [9], [11],  $\lambda^y = e^\alpha \cdot \lambda^O \cdot \lambda^I$ , where

$$\begin{aligned} \log \lambda^O (t | H_t^{y_j}, \Theta) &= \sum_{r=1}^6 \gamma_r^j N_r^{y_j} \\ \log \lambda^I (t | H_t^u, \Theta) &= \sum_{i=1}^{13} \sum_{r=1}^4 \beta_r^{i,j} N_r^{u_i} \end{aligned} \quad (15)$$

where  $H_t^{y_j}$  corresponds to the output neuron's own history, and  $u_i$ , the input, corresponds to the multi-unit spiking activity of the neurons at the  $i$ -th PMv recording channel.  $N_r^{y_j}$  or  $N_r^{u_i}$  is the number of spikes fired by the  $j$ -th M1 neuron or at the  $i$ -th PMv channel in  $[t - r, t - (r - 1)]$  (in ms) respectively ( $r$  varied from 5 to 100 ms), and

$$\Theta_j = \left[ \alpha, \left\{ \gamma_r^j \right\}_{r=1}^6, \left\{ \left\{ \beta_r^{i,j} \right\}_{r=1}^4 \right\}_{i=1}^{13} \right].$$

We arrived at the above choice of covariates and the model structure given in (15) through an iterative procedure of testing and refining GLM models until the models' cross-validated KS plots displayed a high goodness-of-fit for each model [25]. In this analysis, the  $m = 21$  neurons include only those with cross-validated KS statistic  $< 0.2$ .

**2) Clustering**—We then clustered the PPM parameter vectors for each M1 neuron using K-means clustering, as described in section II-C. The average silhouette values were computed for  $K = 2, \dots, 20$ . We chose  $K = 4$  (average silhouette value 0.65) for this analysis by analyzing the KS plots of the resulting clustered models and choosing those with the highest goodness-of-fit. The resulting clusters defined a simple set of physiological

connections between the PMv and M1 neurons. The first cluster contained the input-output model parameters of M1 neurons  $n_1, \dots, n_{12}$ , the second cluster contained those of M1 neuron  $n_{13}$ , the third cluster contained those of M1 neurons  $n_{14}, n_{15}$ , whereas the fourth cluster contained those of M1 neurons  $n_{16}, \dots, n_{21}$ . In this study, there was a reduction of the number of input-output models from 21 to 4, i.e.,  $\rho = 5.25$

**3) Aggregate Input Output Models**—Once the clusters were determined, we estimated new aggregate point process models for each PMv-M1 cluster by taking as inputs and outputs several trials from the PMv and M1, respectively. PPMs of the form (6) and (7) were constructed (Fig. 7). The aggregate IO models were then used for statistical inferences regarding the impact of PMv over the activity in M1, and the differences in the activity of the clusters during the four different tasks were examined [11].

Figs. 8A, ..., D show the average firing rate of the PMv neurons which are seen to have a significant effect (with a confidence of  $< 95\%$ ) on the respective clusters of M1 neurons  $k = 1, \dots, 4$ , during the four different tasks. They also show  $\lambda_k$   $k = 1, \dots, 4$  as estimated on all the trials performed during each task. Interestingly, these show the task specificity of the neurons in the resulting clusters, even though the models did not specifically contain task information.

The M1 neurons in cluster 1 show steady firing throughout the trial during all tasks, from 300ms before the onset of movement to 300ms after. There seems to be no task specificity in these neurons. In Fig. 7A, the average firing rate is seen to be around 20 spikes/s. We also see that only 4 of the PMv channels have a significant impact on the M1 neurons in this cluster, and that this effect is limited to a very slight inhibition or excitation.

The M1 neuron in cluster 2 modulates its activity specific to the task. During the tasks involving the pushbutton and the sphere, the neuron increases spiking prior to movement onset, and again around 200ms after movement onset. However, during the task involving the cylinder as well as the mallet, the spiking of the neuron is seen to decrease around movement onset, and increase after 200ms after onset. This task specificity might arise due to the direction of reach of the primate during tasks involving the pushbutton and sphere (right) as opposed to those involving the cylinder and the mallet (left). This specificity might also be due to the nature of the task itself, i.e. the cylinder and mallet tasks both comprise of pulling a certain object towards the primate. In Fig. 7B, we see that 10 of the PMv channels have a significant impact on the M1 neurons in this cluster, of both an excitatory and inhibitory nature. Note that this effect is more significant than seen in the M1 neurons in cluster 1.

The M1 neurons in cluster 3 also show task specificity. During the pushbutton and the sphere trials, the neurons increase their spiking right after movement onset. During the task involving the cylinder, the neurons increase their spiking after 200ms after onset of movement, whereas during the task involving the mallet, they increase their spiking before movement onset. This difference in activity during tasks might be due to the different directions of reach. We again see significant excitatory and inhibitory effects from 10 PMv channels towards the M1 neurons in this cluster, in fig. 7C.

The M1 neurons in cluster 4 show no task specificity, and display a steady firing throughout the trial during all tasks, of around 30 spikes/s. This is slightly larger than the firing rate of the M1 neurons in cluster 1. In fig. 7D, we see that only 4 of the PMv channels have a significant effect on the activity of neurons in this cluster.

PMv neurons are hypothesized to affect movement during the observation as well as grasping of the target. Here, we capture the effect of the PMv neurons during the observation of the target, as well as during direction-related movements. PMv neurons are known to provide direct connections to the M1 pyramidal neurons, as well as to the interneurons which themselves inhibit the M1 pyramidal neurons. A combination of inhibitory and excitatory effects have been seen on M1 neurons when the PMv neurons were stimulated using transcranial magnetic stimulation [30]–[33]. An inhibition at similar time scales as seen in this study has been specifically noted in the study by Tokuno and Nambu [30]. The net inhibitory effect from several neurons in the PMv to the M1 may be due to the indirect connection to the M1 pyramidal neurons via the M1 interneurons.

In this study, the neurons in PMv channels are seen to have a combination of significant inhibitory as well excitatory effects on the M1 neurons in each cluster, but a higher number of PMv neurons are seen to have a significant effect on the *task-specific* M1 clusters (clusters 2 and 3). This suggests that the PMv spiking plays an integral part in the planning of directed movements. Moreover, we successfully captured the nature of this non-trivial relationship using aggregate PPMs.

## V. DISCUSSION

We propose a method to construct reduced order data-driven predictive models that characterize the effect of spiking activity of neurons in one region of the brain to neurons in another region. The systems identification technique detailed above can be used for any number of neuronal recordings obtained from several regions of the brain, in order to understand the IO dynamics of the structures in question. We applied this method to simulated data as well as primate data from M1, S1 and PMv during different parts of a behavioral task. Both the S1 and the PMv neurons have a combination of inhibitory and excitatory effects on the M1 neurons, and a successful input-output mapping of the relevant structures during specific periods of the behavioral task was built using the aggregate PPMs.

One of the limitations of this method is the need for a substantial amount of data to build aggregate IO models that pass the goodness of fit criteria, especially with an increase in the number of inputs. We also need simultaneously recorded spike trains to be able to build these predictive IO models. However, many of the electrophysiological studies performed satisfy these criteria, i.e. recording a large amount of data and simultaneously from several regions.

In this study, we concentrated on characterizing the relationship between activity in one input region to one output region. However, this method could easily be extended to include several input regions, for example, M1 simultaneously receiving inputs from the PMv, S1 and PMd.

The method detailed in this paper can be used to construct data driven models that provide us with explicit and interpretable information on the spiking activity of groups of output neurons dependent on input neurons. We also gain an insight into the physiological connections between neurons in the input and output regions, without making any assumptions on the underlying structure of these models, apart from the specification of input and output regions. Moreover, the aggregate input-output models are tractable and easy to analyze since they are reduced order models and represent the activity of clusters of neurons. Using these aggregate IO models, we can portray relationships between regions of the brain which are not physically connected, thus summarizing the effect from input neurons connected to the output region even via several synapses and regions. The method is seen to be effective in model reduction, obtaining aggregate models, and quantifying the effects of groups of input neurons on groups of output neurons; and is a key step towards building a computational IO system model of neurons in interconnected brain nuclei.

## Acknowledgments

This work was supported by the Burroughs Wellcome Fund CASI 1007274 and NSF CAREER 1055560 to SVS.

## Biographies



**Shreya Saxena** Shreya Saxena received her B.S. degree in Mechanical Engineering from the Swiss Federal Institute of Technology, Lausanne, Switzerland in 2009; and her M.S. in Biomedical Engineering from Johns Hopkins University in Baltimore MD, in 2011. She is currently pursuing a Ph.D. in the Department of Electrical Engineering and Computer Science at Massachusetts Institute of Technology in Cambridge MA. Her research interests include model estimation and control of neural systems, especially in the field of movement generation and brain machine interface.



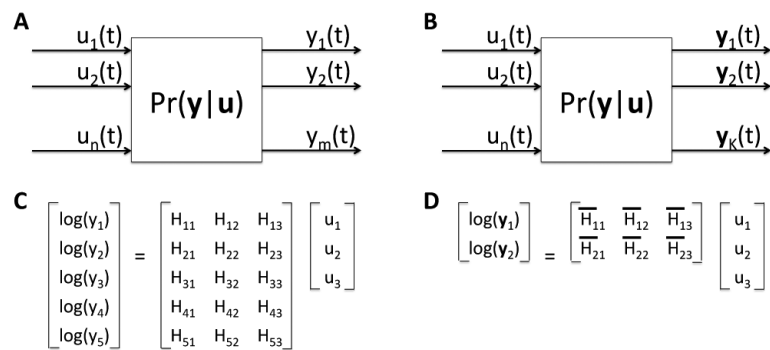
**Sridevi V. Sarma** Sridevi V. Sarma (M'04) received the B.S. degree in Electrical Engineering from Cornell University, Ithaca NY, in 1994; and an M.S. and Ph.D. degrees in Electrical Engineering and Computer Science from Massachusetts Institute of Technology

in, Cambridge MA, in 1997 and 2006, respectively. She was a Postdoctoral Fellow in the Brain and Cognitive Sciences Department at the Massachusetts Institute of Technology, Cambridge, from 2006-2009. She is now an assistant professor in the Institute for Computational Medicine, Department of Biomedical Engineering, at Johns Hopkins University, Baltimore MD. Her research interests include modeling, estimation and control of neural systems. She is a recipient of the GE faculty for the future scholarship, a National Science Foundation graduate research fellow, a L'Oreal For Women in Science fellow, and a recipient of the Burroughs Wellcome Fund Careers at the Scientific Interface Award and the NSF CAREER award.

## REFERENCES

- [1]. Nicolelis MAL, Ghazanfar AA, Faggin BM, Votaw S, Oliveira LMO. Reconstructing the engram: Simultaneous, multisite, many single neuron recordings. *Neuron*. 1997; 18(4):529–537. [PubMed: 9136763]
- [2]. Mollazadeh M, Aggarwal V, Davidson AG, Law AJ, Thakor NV, Schieber MH. Spatiotemporal variation of multiple neurophysiological signals in the primary motor cortex during dexterous reach-to-grasp movements. *Journal of Neuroscience*. 2011; 31(43):15 531–15 543. [PubMed: 21209185]
- [3]. Hashimoto T, Elder CM, Okun MS, Patrick SK, Vitek JL. Stimulation of the subthalamic nucleus changes the firing pattern of pallidal neurons. *Journal of Neuroscience*. 2003; 23:1916–1923. [PubMed: 12629196]
- [4]. Kita H, Tachibana Y, Nambu A, Chiken S. Balance of monosynaptic excitatory and disynaptic inhibitory responses of the globus pallidus induced after stimulation of the subthalamic nucleus in the monkey. *Journal of Neuroscience*. 2005; 25(38):8611–8619. [PubMed: 16177028]
- [5]. Rubin JE, Terman D. High frequency stimulation of the subthalamic nucleus eliminates pathological thalamic rhythmicity in a computational model. *Journal of Computational Neuroscience*. 2004; 16:211–235. [PubMed: 15114047]
- [6]. Feng X, Greenwald B, Rabitz H, Shea-Brown E, Kosut R. Toward closed-loop optimization of deep brain stimulation for parkinson's disease: concepts and lessons from a computational model. *Journal of Neural Engineering*. 2007; 4(2):L14. [PubMed: 17409470]
- [7]. Barbieri R, Quirk MC, Frank LM, Wilson MA, Brown EN. Construction and analysis of non-poisson stimulus-response models of neural spiking activity. *Journal of Neuroscience Methods*. 2001; 105:25–37. [PubMed: 11166363]
- [8]. Czanner G, Eden UT, Wirth S, Yanike M, Suzuki WA, Brown EN. Analysis of between-trial and within-trial neural spiking dynamics. *Journal of Neurophysiology*. 2008; 99:2672–2693. [PubMed: 18216233]
- [9]. Kass RE, Ventura V. A spike train probability model. *Neural Computation*. 2001; 13:1713–1720. [PubMed: 11506667]
- [10]. Paninski L. Maximum likelihood estimation of cascade point-process neural encoding models. *Network: Computation in Neural Systems*. 2004; 15:243–262.
- [11]. Sarma SV, Eden UT, Cheng ML, Williams ZM, Hu R, Eskandar E, Brown EN. Using point process models to compare neuronal activity in sub-thalamic nucleus of parkinson's patients and a healthy primate. *IEEE Transactions on Biomedical Engineering*. 2010; 57:1297–1305. [PubMed: 20172804]
- [12]. Truccolo W, Eden UT, Fellows MR, Donoghue JP, Brown EN. A point process framework for relating neural spiking activity for spiking history, neural ensemble and extrinsic covariate effects. *Journal of Neurophysiology*. 2005; 93:1074–1089. [PubMed: 15356183]
- [13]. Cox, DR.; Isham, V. *Point Processes*. CRC; Boca Raton, FL: 2000.
- [14]. Snyder, DL.; Miller, MI. *Random Point Processes in Time and Space*. Springer; New York, NY: 1991.

- [15]. Brown, EN.; Barbieri, R.; Eden, UT.; Frank, LM. Computational Neuroscience: A Comprehensive Approach (Feng, J.). CRC; London: 2003. Likelihood methods of neural data analysis; p. 253-286.ch. 9
- [16]. McCullagh, P.; Nelder, JA. Generalized Linear Models. 2nd. Chapman & Hall / CRC; Boca Raton, FL: 1989.
- [17]. Seber, GAF. Multivariate Observations. John Wiley & Sons, Inc.; Hoboken, NJ: 1984.
- [18]. Rousseeuw PJ. Silhouettes: A graphical aid to the interpretation and validation of cluster analysis. *Journal of Computational and Applied Mathematics*. 1987; 20:53–65.
- [19]. Saxena, S.; Santaniello, S.; Montgomery, EB.; Gale, JT.; Sarma, SV. Point process models show temporal dependencies of basal ganglia nuclei under deep brain stimulation. *Proc. 32nd IEEE EMBS Conference; Buenos Aires, AR*. 2010.
- [20]. Santaniello, S.; Gale, JT.; Montgomery, EB.; Sarma, SV. Modeling the motor striatum under deep brain stimulation in normal and MPTP conditions. *Proc. 32nd IEEE EMBS Conference; Buenos Aires, AR*. 2010. p. 2065-2068.
- [21]. Humphries MD. Spike-train communities: Finding groups of similar spike trains. *Journal of Neuroscience*. 2011; 31(6):2321–2336. [PubMed: 21307268]
- [22]. Brown EN, Barbieri R, Ventura V, Kass RE, Frank LM. The time-rescaling theorem and its application to neural spike train data analysis. *Neural Computation*. 2002; 14:325–346. [PubMed: 11802915]
- [23]. Sarma SV, Nguyen DP, Czanner G, Wirth S, Suzuki W, Wilson M, Brown E. Computing confidence intervals for point process models. *Neural Computation*. 2011 Epub ahead of print.
- [24]. Aggarwal, V.; Kerr, M.; Davidson, A.; Davoodi, R.; Loeb, G.; Schieber, M.; Thakor, N. Cortical control of reach and grasp kinematics in a virtual environment using musculoskeletal modeling software. *Proc. 5th International IEEE EMBS Conference on Neural Engineering; Cancun, Mexico*. 2011.
- [25]. Johnson, NL.; Kotz, S. Distributions in Statistics. Continuous Univariate Distributions - 2. Wiley; New York: 1970.
- [26]. Matyas F, Sreenivasan V, Marbach F, Wacongne C, Barsy B, Mateo C, Aronoff R, Petersen CCH. Motor control by sensory cortex. *Science*. 2010; 330:1240–1243. [PubMed: 21109671]
- [27]. Rocco-Donovan M, Ramos RL, Giraldo S, Brumberg JC. Characteristics of synaptic connections between rodent primary somatosensory and motor cortices. *Somatosensory and Motor Research*. 2011; 28(3-4):63–72. [PubMed: 21879990]
- [28]. Mao T, Kusefoglou D, Hooks BM, Huber D, Petreanu L, Svoboda K. Long-range neuronal circuits underlying the interaction between sensory and motor cortex. *Neuron*. 2011; 72(1):111–123. [PubMed: 21982373]
- [29]. Chagnac-Amitai Y, Connors BW. Horizontal spread of synchronized activity in neocortex and its control by gaba-mediated inhibition. *Journal of Neurophysiology*. 1989; 61(4):747–58. [PubMed: 2542471]
- [30]. Tokuno H, Nambu A. Organization of nonprimary motor cortical inputs on pyramidal and nonpyramidal tract neurons of primary motor cortex: An electrophysiological study in the macaque monkey. *Cerebral Cortex*. 2000; 10(1):58–68. [PubMed: 10639396]
- [31]. Baumer T, Schippling S, Kroeger J, Zittel S, Koch G, Thomalla G, Rothwell J, Siebner H, Orth M, Mnchau A. Inhibitory and facilitatory connectivity from ventral premotor to primary motor cortex in healthy humans at rest - a bifocal TMS study. *Clinical Neurophysiology*. 2009; 120(9): 1724–1731. [PubMed: 19683960]
- [32]. Prabhu G, Shimazu H, Cerri G, Brochier T, Spinks RL, Maier MA, Lemon RN. Modulation of primary motor cortex outputs from ventral premotor cortex during visually guided grasp in the macaque monkey. *The Journal of Physiology*. 2009; 587(5):1057–1069. [PubMed: 19139043]
- [33]. Davare M, Lemon R, Olivier E. Selective modulation of interactions between ventral premotor cortex and primary motor cortex during precision grasping in humans. *The Journal of Physiology*. 2008; 586(11):2735–2742. [PubMed: 18403420]

**Fig. 1.**

A) Original system of inputs  $u_i$  and outputs  $y_j$ ,  $i \in 1, \dots, n, j \in 1, \dots, m$ . B) Reduced system of inputs  $u_i$  and outputs  $y_k$ ,  $i \in 1, \dots, n, k \in 1, \dots, K, K \leq m$ . C) and D) show a transfer matrix representation of these IO systems, with  $n = 3, m = 5, K = 2$ .

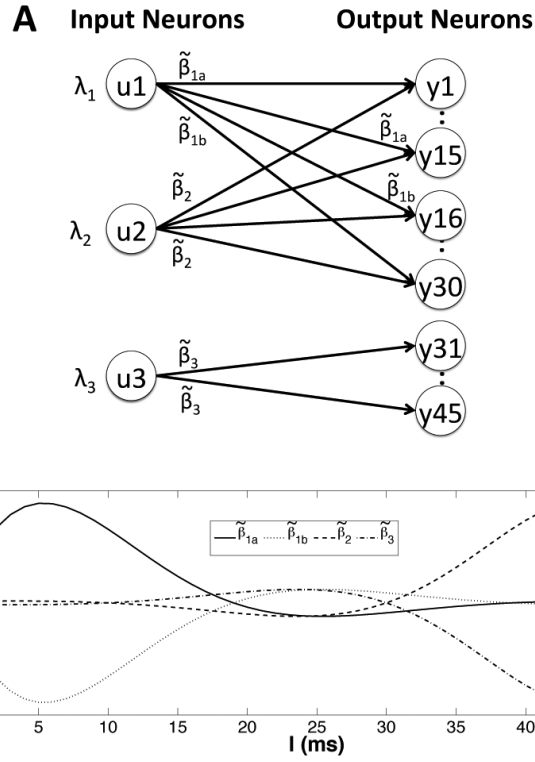


**Fig. 2.** A) A schematic of the functions with which input neurons have an effect on output neurons. Note that  $y_1, \dots, y_{30}$  are simultaneously affected by  $u_1$  and  $u_2$ , whereas  $y_{31}, \dots, y_{45}$  are only affected by  $u_3$ . B) The four functions denoting the propensity with which the output neuron spikes at time  $t$  given that input neuron spiked  $t - l$  ms ago.

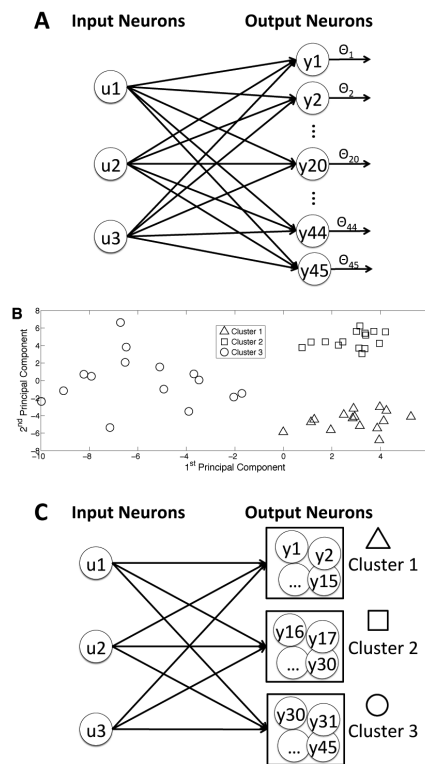


**Fig. 3.** Clustering Analysis. A) Schematic of individual IO model parameters. B) 1st and 2nd principal components of the parameter vectors estimated. Note that the principal components visually separate out  $\Theta_1, \dots, \Theta_{15}, \dots, \Theta_{16}, \dots, \Theta_{30}$ , and  $\Theta_{31}, \dots, \Theta_{45}$ . C) Schematic of aggregate IO models after model reduction via K-means clustering.

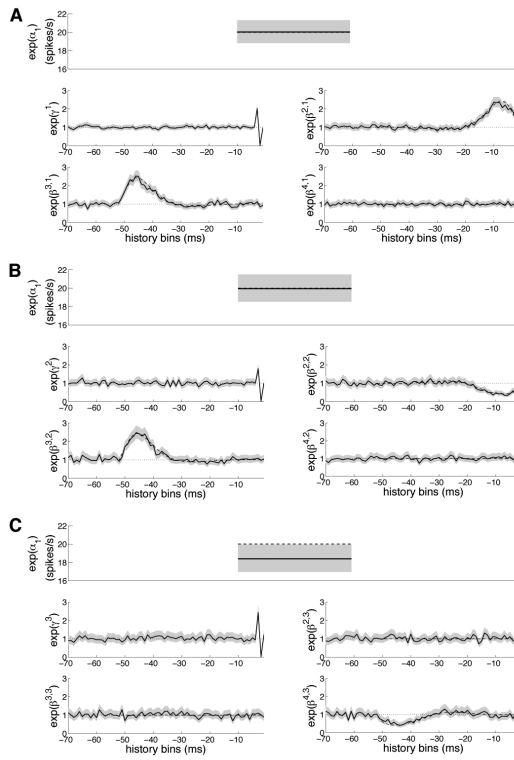


**Fig. 4.** Aggregate IO Model Parameters. A)  $\exp(\bar{\Theta}_1)$ , representing a model of the output neurons  $y_1, \dots, y_{15}$ . B)  $\exp(\bar{\Theta}_2)$ , representing a model of the output neurons  $y_{16}, \dots, y_{30}$ . C)  $\exp(\bar{\Theta}_3)$ , representing a model of the output neurons  $y_{31}, \dots, y_{45}$ . The 95% confidence bounds for the model parameters are depicted in grey around the parameters. The relevant  $\exp(\tilde{\beta}_i)$  are shown in dashed lines.

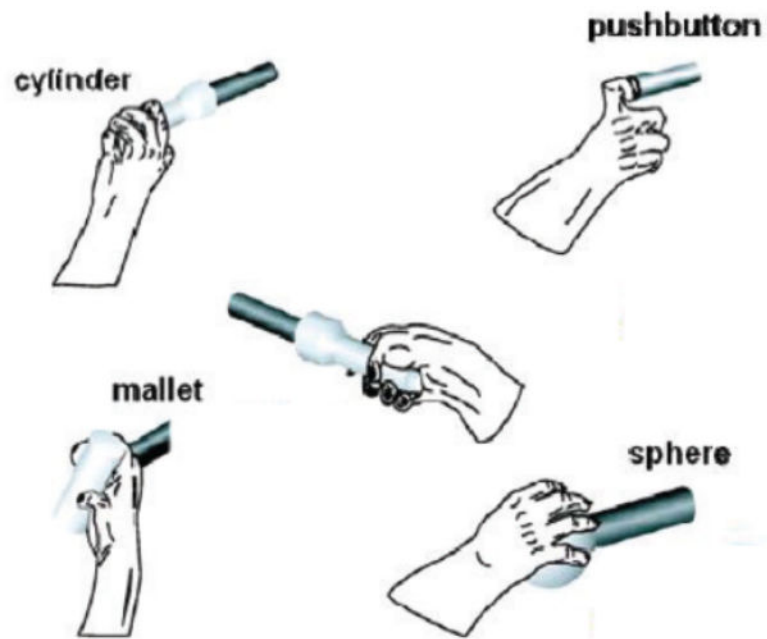


**Fig. 5.** Simultaneous neural activity was recorded from a non-human primate as it reached towards and manipulated four different objects in space.

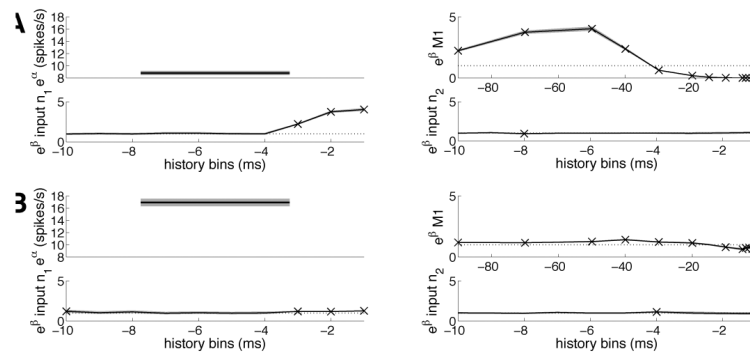


**Fig. 6.** Aggregate IO Model Parameters. A)  $\exp(\bar{\Theta}_1)$ , representing a model of the output neurons  $n1, \dots, n12$ . B)  $\exp(\bar{\Theta}_2)$ , representing a model of the output neuron  $n13$ . The 95% confidence bounds for the model parameters are depicted in grey around the parameters. The crosses refer to those parameters which are significantly different from 1.

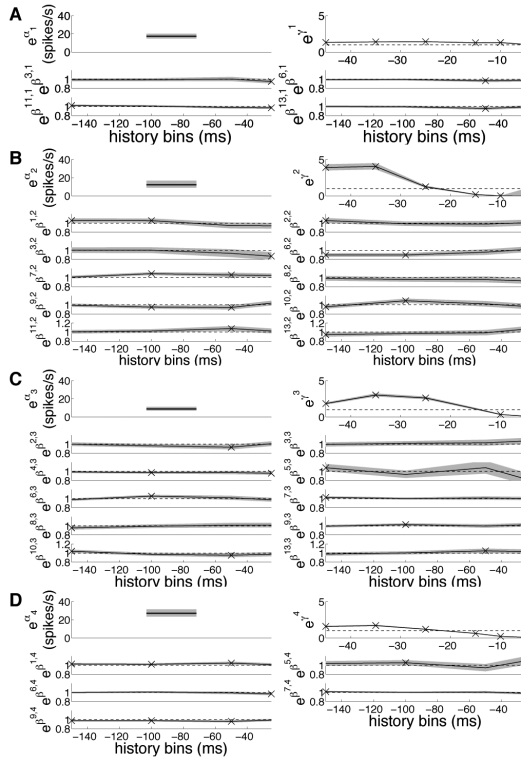


**Fig. 7.** Aggregate IO Model Parameters. A)  $\exp(\bar{\Theta}_1)$ , representing a model of the output neurons  $n1, \dots, n12$ . B)  $\exp(\bar{\Theta}_2)$ , representing a model of the output neuron  $n13$ . C)  $\exp(\bar{\Theta}_3)$ , representing a model of the output neurons  $n14, n15$ . D)  $\exp(\bar{\Theta}_4)$ , representing a model of the output neurons  $n16, \dots, n21$ . The 95% confidence bounds for the model parameters are depicted in grey around the parameters. The parameters that are significantly above or below 0 are depicted by crosses. Only the inputs with at least one significant parameter are shown.

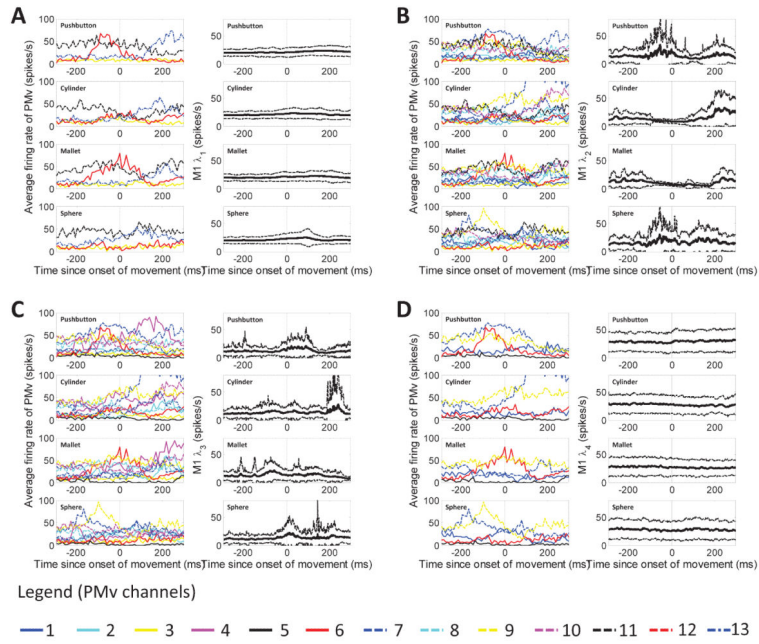


**Fig. 8.** A) , B) , C) , D) The average firing rate at the PMV channels which are shown to have a significant effect (with a confidence of  $< 95\%$ ) on the respective clusters of M1 neurons  $k = 1, \dots, 4$ , during the four different tasks, on the left (color version available online).  $\lambda_k$   $k = 1, \dots, 4$  as estimated on all the trials performed during each task,  $\pm$  one standard deviation in dashed lines, on the right.